

AN ABSTRACT OF THE THESIS OF

James Orrin Paumier for the degree of Master of Science
in Atmospheric Sciences presented on 5 March 1981

Title: Penetrative Elements at the Top of the Atmospheric
Mixed Layer

Abstract approved: Redacted for Privacy

High resolution data of moisture, temperature and wind velocity collected by aircraft during the 1975 Air Mass Transformation Experiment (AMTEX '75) provide information for detailed investigations of the phenomena occurring at the top of a cloud-topped mixed layer.

Joint frequency diagrams of humidity and temperature reveal that for parts of the record the coldest temperatures occur in air near saturation while drier air or air with substantial liquid water is warmer. This suggests the possible occurrence of cloud-top entrainment instability (Deardorff, 1980).

Using humidity as an indicator, the flight record is systematically searched for penetrative mixed layer elements and pockets of dry air penetrating into cloudy air (wisps). The separate phenomena are then composited to produce an "average" wisp and penetrating element. The composites show evidence of net cooling due to evaporation downstream from the penetrating element and upstream from the

wisps. Sinking motion is associated with the cold temperatures. These results suggest the interaction of shear, penetrating elements and wisps, and the existence of cloud-top entrainment instability.

Penetrative Elements at the Top of the
Atmospheric Mixed Layer

by

James Orrin Paumier

A THESIS

submitted to

Oregon State University

in partial fulfillment of

the requirements for the

degree of

Master of Science

Commencement June 1981

APPROVED:

Redacted for Privacy

Associate Professor of Atmospheric Sciences
in charge of major

Redacted for Privacy

Chairman of the Department of Atmospheric Sciences

Redacted for Privacy

Dean of Graduate School

Date thesis is presented 5 March 1981

Typed by Karen Borgen for James Orrin Paumier

ACKNOWLEDGEMENTS

I would like to express my gratitude to my major professor, Prof. Larry Mahrt, for his patience and support while I worked on my thesis; to thank Prof. J.W. Deardorff, Prof. S.K. Esbensen, Prof. C.A. Paulson and Prof. C.K. Sollitt for their suggestions and criticisms; and to thank others in the Department for their helpful comments. I would also like to thank the Oregon State University Milne Computer Center for computing time for the necessary analyses during periods when I had no research support. This research was supported, in part, by Grant ATM 79-10042 from the Global Atmospheric Research Program of the National Science Foundation.

TABLE OF CONTENTS

I. Introduction.....	1
II. Synoptic Conditions and Data.....	3
Synoptic Conditions.....	3
Data.....	4
III. Cloud-top Entrainment Instability (CEI).....	9
IV. Phenomena Related to CEI.....	28
Composite Penetrative Mixed Layer Elements.....	30
Composite Wisp.....	31
Composite Transitions.....	32
V. Summary.....	40
VI. Bibliography.....	42

LIST OF FIGURES

<u>Figure</u>	<u>Page</u>
1 Schematic representation of aircraft flight and humidity time series at cloud-top	5
2 DMSP satellite photograph on 16 February 1975 at 0255Z (1155 JST)	7
3 Possible results of mixing a free flow and mixed layer parcel	10
4a Joint frequency diagram of humidity, q , and temperature, θ_v , for entire EW flight	19
4b As in 4a except for first third of flight (EW1)	20
4c As in 4a except for second third of flight (EW2)	21
4d As in 4a except for final third of flight (EW3)	22
5a As in 4a except for entire NS flight	24
5b As in 5a except for first third of flight (NS1)	25
5c As in 5a except for second third of flight (NS2)	26
5d As in 5a except for final third of flight (NS3)	27
6 Composite penetrative mixed layer element	34
7 Penetrative element with highest central moisture	35
8 Composite wisp	36
9 Composite moist-to-dry transition	37
10 Composite dry-to-moist transition	38
11 PMLE and wisp composite plotted on the q - θ_v diagram	39

PENETRATIVE ELEMENTS AT THE TOP OF THE
ATMOSPHERIC MIXED LAYER

I. INTRODUCTION

Numerous statistical studies of the top of the atmospheric boundary layer have been conducted, both observational (e.g. Jensen and Lenschow, 1978) and modelling (e.g. Ball, 1960; Lilly, 1968; Deardorff, 1974 and Stull, 1976). However, little attention has been devoted to the phenomenological study of the top of the boundary layer. This study attempts to identify important phenomena and physical interactions at the top of an atmospheric boundary layer using high resolution aircraft data (every 5 m) collected in the Air Mass Transformation Experiment (AMTEX) during a cold air outbreak over the East China Sea.

The top of the boundary layer may be capped by an inversion, separating a relatively non-turbulent free flow above from a much more turbulent mixed layer below. Across this zone vertical shear in the horizontal wind velocity may exist and strongly influence circulations in the interfacial region. The top of the cloud, like the top of any mixed layer, may be characterized by the occurrence and interaction of various phenomena: 'hummocks' (Browning et al., 1973), convective penetrating elements (Grant, 1965; Palmer et al., 1979) which may be overturning and engulfing free flow air (Carson and Smith, 1974) due to the shear across the interface, shear driven eddies on the scales of the boundary layer or inversion thickness, and gravity waves (Palmer et al., 1979). These mechanisms contribute to the entrainment of warm, dry free flow air into the cool, moist cloud

layer.

Pockets of engulfed dry air can be cooled by evaporation of liquid water when mixed with the cloud air. If the resulting mixture is negatively bouyant with respect to the cloud air, it can sink farther into the cloud. This instability mechanism has been examined in mixed layer growth models (Lilly, 1968) and modelling of stratiform cloud (Paltridge, 1974; Randall, 1980; Deardorff, 1980). This instability is thought to lead to the breakup of stratocumulus clouds; however, there is no direct observational evidence that this occurs. It is the purpose of this paper to provide observational evidence of the existence of the instability and to examine its occurrence in relation to some of the other phenomena observed at the top of the atmospheric mixed layer.

II. SYNOPTIC CONDITIONS AND DATA

A. Synoptic Conditions

The Kuroshio, a warm ocean current in the western North Pacific, flows northeastward along the edge of the continental shelf with a sea surface temperature in excess of 20°C even during the winter months. In the Yellow Sea, more than 700 km to the northwest and just off the coast of China, sea surface temperatures are observed to be less than 10°C, resulting in a large sea surface temperature gradient. Cyclones, fronts, and frontogenesis are frequently observed in this region (Reed, 1960). After the passage of a cyclone, winds in the boundary layer are northerly or northwesterly, and very cold air from the Asian interior flows over the Kuroshio. This air is rapidly modified by strong upward heat flux from the much warmer water.

A depression east of Taiwan developed on the morning of 13 February 1975 with a central pressure of 1016 mb. This system deepened (1004 mb) and was located northwest of Naha, Okinawa the following morning. A cold front developed and moved through the AMTEX data network at this time. After the passage of the cold front on 14 February, cold air from the Asian continent flowed out over the Kuroshio. On 15 February the low moved to 900 km east of Japan and deepened to 982 mb with the cold front extending to 800 km southeast of Okinawa. Mesoscale cellular convection (MCC) was present over the East China Sea and a strong capping inversion separated the free flow and the mixed layer. The low continued to deepen until a central pressure of 956 mb was reached.

The cold air outbreak persisted through 16 February before beginning to weaken on 17 February. Lenschow and Agee (1976) and Ninomiya (1976) have described the synoptic conditions for AMTEX '75 in more detail.

B. Data

From 15 February to 28 February 1975 the National Center of Atmospheric Research (NCAR) Electra aircraft made several flights over the East China Sea while participating in AMTEX. For about 25 minutes near mid-day (0455Z) on 16 February, part of the period of the cold air outbreak, the Electra flew at 854 mb at an approximate speed of 100 ms^{-1} . The flight was conducted at the top of the atmospheric mixed layer and was the only extended flight at the mixed layer top during AMTEX '75. Due to the undulating nature of the inversion, the aircraft alternately intersected the mostly cloudy mixed layer air and free flow air, as depicted in Figure 1. A 65 km flight leg from south to north (NS flight) at $\sim 125^\circ \text{ E}$ was followed by a 65 km flight from west to east (EW flight) at $\sim 28.7^\circ \text{ N}$. Figure 2, a DMSP satellite photograph taken at 0255Z on 16 February, shows the location of the flight legs north of the ship Keifu Maru, the array of land and ship observation stations and, the location of the Kuroshio. The MCC patterns are very prominent in this photograph.

Approximately two hours prior to these horizontal flights and over the observation ship Keifu Maru, the aircraft made a vertical traverse through the mixed layer and into the overlying free flow. The horizontal wind profile, constructed from the aircraft sounding, shows the winds in the boundary layer to be northerly and to be

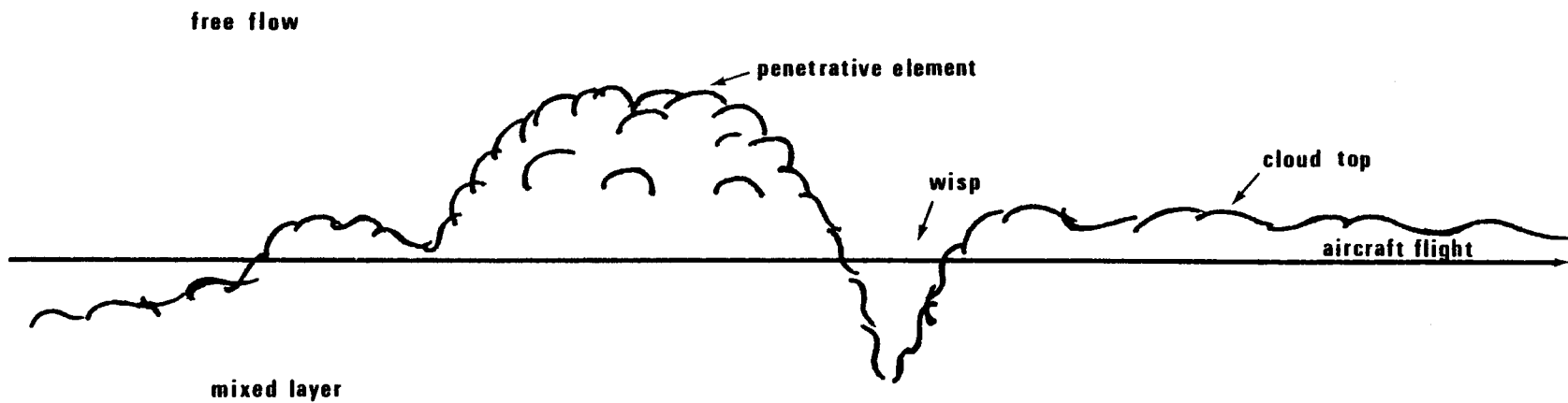
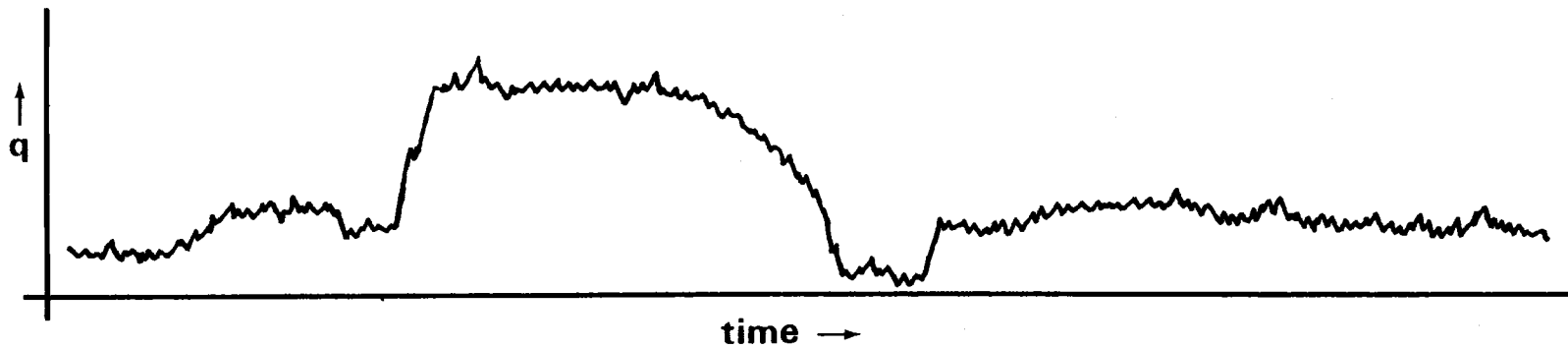
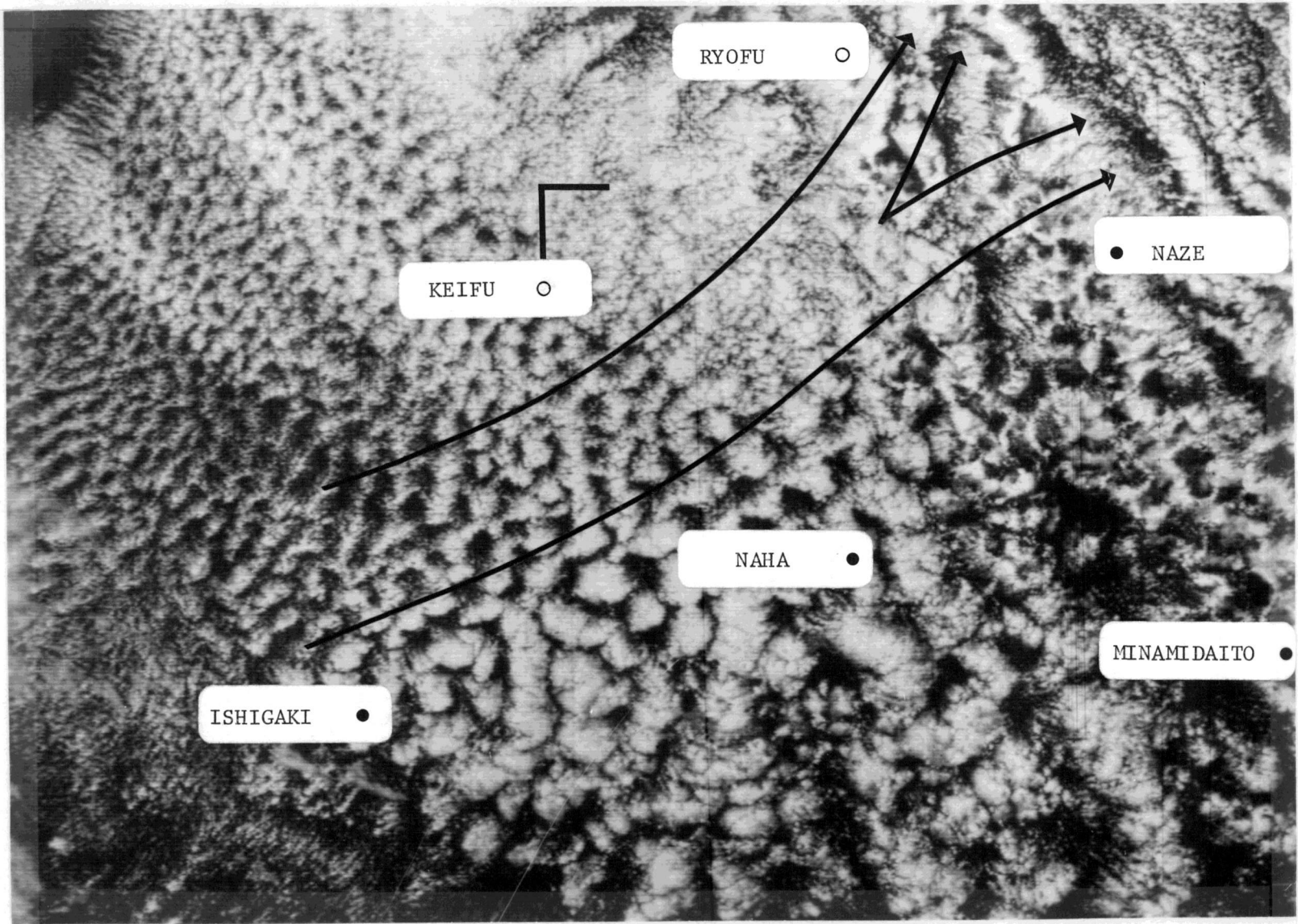


Figure 1. Schematic diagram of aircraft flight at the top of the atmospheric mixed layer (854 mb). A rough schematic representation of the humidity time series for the flight is shown above.

Figure 2. DMSP satellite photograph taken at 0255Z (1155 JST) on 16 February 1975. Heavy lines above ship Keifu is the approximate location of the two flight legs. The photograph was taken two hours before the time of the flights. The Kuroshio is indicated by the arrows. Ship observation stations are indicated by open circles (o); land stations are indicated by black circles (•).



northwesterly above the boundary layer. Lenschow (1972) reports that the winds above the boundary layer during periods of cold air outbreaks tend to be more westerly, as is the case here.

Variables used in the analyses, which were sampled at a rate of 50 observations per second and reduced to 20 observations per second (every 5 m), are absolute humidity measured by a microwave refractometer, temperature measured by a Rosemount resistance wire thermometer, and the vertical component of wind measured by a vane. Lenschow and Agee (1976) reported on the data collection network and Wyngaard et al. (1978) reported on the aircraft instrumentation.

Before the analyses were performed, absolute humidity was converted to specific humidity, q , and the temperature was adjusted for dynamic heating of the wire (Wyngaard et al., 1978). The reliability of the humidity observations was verified by comparing moisture-temperature joint frequency diagrams of the various humidity instruments that were used on the flights. The pattern of the observations agreed well between instruments, although one, the Lyman-Alpha hygrometer, yielded some erroneous values.

The Rosemount thermometer and its housing are subject to wetting while flying through a cloud, although the sensor is partially protected by a 90° bend in the housing (Lenschow and Pennell, 1974). When the aircraft returns to unsaturated air, evaporative cooling of the sensor or the housing can cause an apparent temperature decrease on the order of $1 - 2^\circ\text{C}$ (Heymsfield et al., 1978). Jensen and Lenschow (1978), using much of the same data used here, reported no obvious indications of wetting in the temperature observations.

III. CLOUD-TOP ENTRAINMENT INSTABILITY (CEI)

Water vapor is less dense than dry air and the density difference must be accounted for when considering the bouyancy of a parcel of air. This can be accomplished by considering two separate gas constants, one for dry air and one for moist air, or by introducing a fictitious "virtual" temperature and using only the dry gas constant. As is usual we adopt the latter method and the temperature observations are converted to virtual potential temperature, θ_v . The effects of liquid water, q_l , are not included in defining θ_v due to incorrect calibration of the instrument. By using a pseudo-adiabatic diagram, the amount of liquid water resulting from lifting a parcel from 900 mb to 854 mb is about 0.4 gkg^{-1} and a parcel lifted from 1000 mb to 854 mb about 0.75 gkg^{-1} of liquid water. These calculations neglect mixing during the ascent and, therefore, are overestimates.

The saturation specific humidity, q_s , is here a function only of temperature since the flight legs occurred at constant pressure (854 mb). It can be computed by using the Clausius-Clapeyron equation or Tetens' (1930) empirical relationship, both of which are non-linear. For the small range of temperatures encountered here, the resulting curve is nearly linear.

If two distinct and fixed parcels, one from the mixed layer and one from the overlying free flow, are mixed in various proportions, one of three possible mixing pathways may result, as depicted in Figure 3. Mixtures with mostly cloud air are nearest to the mixed layer parcel. The proportions of cloud air to free flow air, when

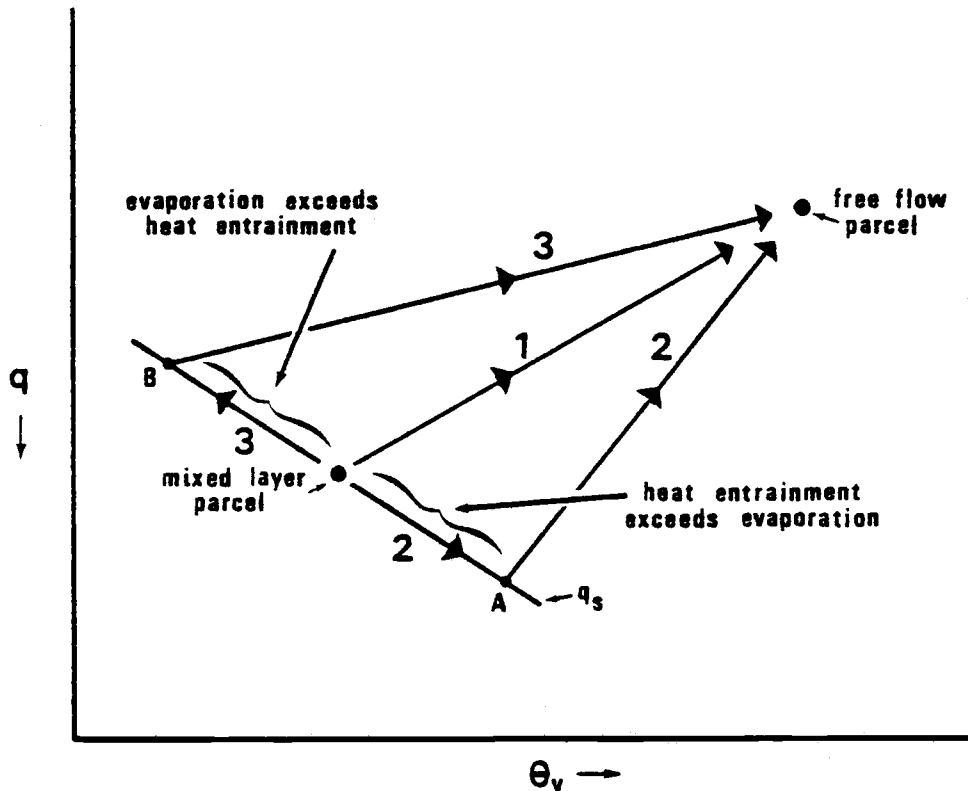


Figure 3. Possible mixing pathways when a mixed layer parcel and free flow parcel are mixed in various proportions at constant pressure. The saturation curve is denoted by q_s ; path 1 represents mixing when no liquid water is present in the mixed layer parcel, whereas paths 2 and 3 are representative of mixing with cloud air. A and B are the points where all the liquid water has evaporated. Arrows on the paths indicate the case of a cloudy parcel entraining an increasing amount of free flow air. Arrows in the opposite direction could indicate, for example, an entraining free flow element being diluted with increasing amounts of cloud air.

all liquid water has evaporated (A and B), depends on the initial properties, i.e. q , θ_v and liquid water, q_l , of the two parcels.

Pathway 1 describes the mixing when no liquid water is present to evaporate, the result being a weighted average of q and θ_v of the two parcels. Paths 2 and 3 describe the mixing when liquid water is present in the mixed layer parcel. Path 2 is produced when the warming due to entrainment of sensible heat exceeds the loss due to evaporation. Assuming constant pressure, q_s increases as temperature increases, corresponding to the evaporation of liquid water in the parcel mixture. Once all the water is evaporated (at pt. A in Figure 3) drying of the mixture occurs. Pathway 3 results when evaporative cooling exceeds the entrainment of free flow sensible heat. The parcel dries but remains saturated ($q = q_s$) until all the liquid water is evaporated (pt. B) and then subsequently warms with further mixing, resulting in a temperature minimum.

The air at the shift from cooling to warming, pt. B in Figure 3, is colder than the average temperature of the surrounding air and, thus, negatively bouyant. The cold mixture sinks within the cloud, generating shear and turbulent kinetic energy and possibly enhancing entrainment of additional dry air. This possibility is known as cloud-top entrainment instability (CEI) (Deardorff, 1980).

To determine the results of mixing a hypothetical mixed layer parcel and free flow parcel in various proportions, we use Deardorff's (1976) empirical formulation for q_s . As an example we use the values of temperature and humidity obtained from the aircraft sounding discussed earlier and choose mixed layer air representative of 1000 mb

($\theta = 281$ K and $q = 4.25$ gkg^{-1}), lift it 854 mb and then mix it with free flow air representative of air just above the clouds ($\theta = 286$ K and $q = 1.3$ gkg^{-1}). The liquid water that condenses during the lifting amounts to about 0.7 gkg^{-1} . This produces the theoretical entrainment curve with a temperature minimum, shown in Figure 4a, as in pathway 3. When the mixture is less than 25% free flow ($0 < E < .25$), the mixing yields a new cooling. With further mixing of free flow ($E > .25$) there is a net warming since all the liquid water is evaporated.

The effects of cloud-top radiative cooling are possibly important but are uncertain in this study, since there is no information on the radiative flux divergence at the time of the flights. Theoretical and observational studies indicate that the cooling rates can vary greatly. Roach and Slingo (1979) find cooling rates as large as several degrees per hour; Goisa and Shoshin (1969) and Zdunkowski *et al.* (1974) report values near -2°C/hr ; Stephens *et al.* (1978) found that shortwave heating is important and must be taken into account with the resulting cooling rates as little as a few tenths of a degree per hour. For mixed layer penetrative motions with time scales on the order of 10 min. a parcel could cool between a few hundredths of a degree to almost 1 K. The cooling observed in this study is larger so that evaporative cooling must be important.

The actual behavior of the thermodynamic state of the flow at the top of the atmospheric mixed layer is illustrated by the $q - \theta_v$ joint frequency diagrams for the EW and NS flight legs (Figures 4a and 5a, resp.). These diagrams are constructed by dividing the q -axis into intervals 0.1 gkg^{-1} wide and the θ_v -axis into intervals 0.25 K wide,

then tallying each observation into the appropriate cell. Cells with ten or more observations are within the solid line, 25 or more are within the dashed line, and 100 or more are within the dotted lines. The total number of observations for each leg is approximately 13,000.

From these diagrams it is evident that there are two major populations at the top of the mixed layer -- a warm, dry regime representing the free flow and a cool, moist regime representing the mixed layer. Intermediate values can be thought of as a mixture between these two states. Since the aircraft is flying at constant pressure, the presence of the two populations indicates that the inversion interface is undulating.

The distribution of the cool, moist values is indicative of evaporative cooling, particularly for cells with 25 or more observations on the EW flight leg.

Some of the moisture values for both legs are greater than saturation. Since the saturated air should collapse along a line described by the Clausium-Clapeyron relationship, instrument error could be responsible for the moisture values greater than saturation. In addition the moist maxima on the north-south flight do not align with the saturation curve, indicating a calibration error in the moisture sensor. This prohibits a quantitative investigation of the flight record, as is done in section IV, on the north-south.

The full flight diagrams are instructive but do not show important horizontal variations of the flow behavior. The east-west and north-south flights can be more or less naturally divided into three equal, non-overlapping segments approximately 20 km long, as in Jensen and

Lenschow (1978). The second segment on the east-west flight (EW2) and the third segment on the north-south flight (NS3) consist mostly of free flow air. Segment three of the east-west flight (EW3) and the second segment of the north-south flight (NS2) are observations of mixed layer air. The remaining segment on each flight (EW1 and NS1) represents a combination of free flow and mixed layer air where the aircraft penetrated the undulating interface several times. The observations in each of these segments are tallied as before.

In the two free flow segments, EW2 and NS3, (Figures 4c and 5d), there is no active evaporative cooling and cloud-top entrainment instability at flight level.

In the east-west undulating segment (EW1), the possibility of net evaporative cooling and CEI is suggested, whereas in the undulating north-south segment (NS1) such evidence is missing. EW1 (Figure 4b) could be characteristic of either path 2 or path 3 (in Figure 3) or both, since there is a discontinuity in observations ($n < 10$) in the cold portion. Inspection of the coldest values reveals that most of these occur at or very close to the downstream boundaries of large ($\sim 1 \text{ gkg}^{-1}$) horizontal decreases of moisture. Therefore, it is possible that evaporative cooling dominates at these locations but the existence of CEI is still tentative. Here "downstream" refers to the east edges of a penetrating mixed layer element. Since the free flow has a stronger westerly component than does the mixed layer, it is expected to flow around or over the slower moving mixed layer air.

The north-south undulating segment (NS1), shown in Figure 5b, is similar to EW1 except that a continuum of observations from cold to

warm exists. It resembles the warming and moistening path (2) in Figure 3 and, thus, CEI probably does not occur here at flight level. Inspection of the coldest values reveals that they occur largely in a short mixed layer subsegment and are not systematically associated with any prominent north-south horizontal moisture gradients. The coldest air is probably associated with thermals that have become saturated (Lenschow and Stephens, 1980) rather than CEI.

Both mixed layer segments, EW3 and NS2 shown in Figures 4d and 5c, (resp.), are characteristic of evaporative cooling (pathway 3). As noted earlier there is an instrument error for NS2, since many of the humidity values are greater than saturation. Nevertheless, trends in the data suggest the occurrence of CEI.

The mixed layer segment of the east-west flight (EW3) provides strong support for CEI. The evaporative cooling elbow is very prominent, especially when the number of observations exceeds 25 per cell. Some of the coldest air occurs with downstream jumps in moisture (moist-to-dry), when such transitions are definable. Most of the remaining cold air occurs in short subsegments of mixed layer air. The downstream transition zones favor mixing of free flow and cloud air. Air flowing over or around the mixed layer air may form a wake at the downstream edge, enhancing the mixing of the two types of air, as will be seen in Section IV. Thus these locations are favorable to the occurrence of CEI.

Since the aircraft flew at only one level here, it is not clear if the above observations suggest that CEI occurred generally in the lower portions of the entrainment layer or occurred in regions where

the mixed layer is deepest. The latter possibility could occur if CEI systematically led to enhanced entrainment and mixed layer growth.

Nearly saturated air ($2.0 < q < 3.0 \text{ gkg}^{-1}$) in EW3, probably occurring immediately outside the cloud boundary in unsaturated air, is exceptionally cold when compared, for example, to nearly saturated air in segment EW1 or when compared with the temperatures expected for these moisture values based on the $q-\theta_v$ trend established in the drier air (see region A, Figure 4c). This cold anomaly could be due to the diffusion of liquid water droplets into the unsaturated near-cloud environment and the subsequent cooling due to evaporation of the cloud droplets into unsaturated air.

Such a wet-bulb process is described by the relation

$$(T - T')(c_p + wc_{pv}) + (w' - w)L \quad (1)$$

where T is the temperature of the air parcel, T' is the temperature after the evaporation of water, c_p is the specific heat of dry air at constant pressure, c_{pv} is the specific heat of water vapor at constant pressure, w' is the mixing ratio after evaporation, w is the mixing ratio of the parcel prior to evaporation and L is the latent heat of evaporation. The influence of the temperature difference between the air parcel and the water droplets is neglected. The term wc_{pv} is small compared to c_p and if we assume that $w \approx q$, the following equation for T' results

$$T' = T - (q' - q)L/c_p \quad (2)$$

If evaporation continues until saturation, then q' is the saturation

specific humidity and T' is the wet-bulb temperature, T_w .

A line relating T' and q' can be computed by choosing representative values of q and T for the free flow; we increase the specific humidity (q') corresponding to the evaporation of liquid water into the dry air and determine the resulting temperature (T'). Values of $q = 1.3 \text{ gkg}^{-1}$ and $\theta_v = 286 \text{ K}$ are chosen to start the process, the same free flow values used to determine the theoretical entrainment curve earlier. The results are plotted on the q - θ_v frequency diagram EW3 (Figure 4d). Since the line passes through the anomalous cold values, a wet-bulb process becomes a possible explanation.

This process differs from the cloud-top entrainment instability mechanism. The entrainment instability requires the mixing of two air parcels with different properties, one parcel containing liquid water. The wet-bulb process requires only one parcel with cloud droplets diffused into it. Murray and Koenig (1972), in their numerical experiments of cumulus convection, crudely partition the diffusion of the liquid water into cloud water (droplets) and precipitation water (raindrops). They assume that the turbulent transport of the large drops is negligible and is finite for the droplets. It is possible, then, that the inertia of the droplets carries them from the turbulent cloudy air into the unsaturated near-cloud environment, as indicated by Murray and Koenig.

From Figure 4d it appears that the wet-bulb temperature is not realized. The temperatures computed by this process are too cold for the higher moisture values. What appears to be occurring is that the liquid water droplets are diffused into the near-cloud environment, the

parcel cools by the wet-bulb process and, before reaching T_w , is entrained into the mixed layer where cloud-top entrainment instability may occur. The point of entrainment is approximately where the line describing the wet-bulb process diverges from the observations, which in this case is near $\theta_v = 283$ K (labelled A on Figure 4d).

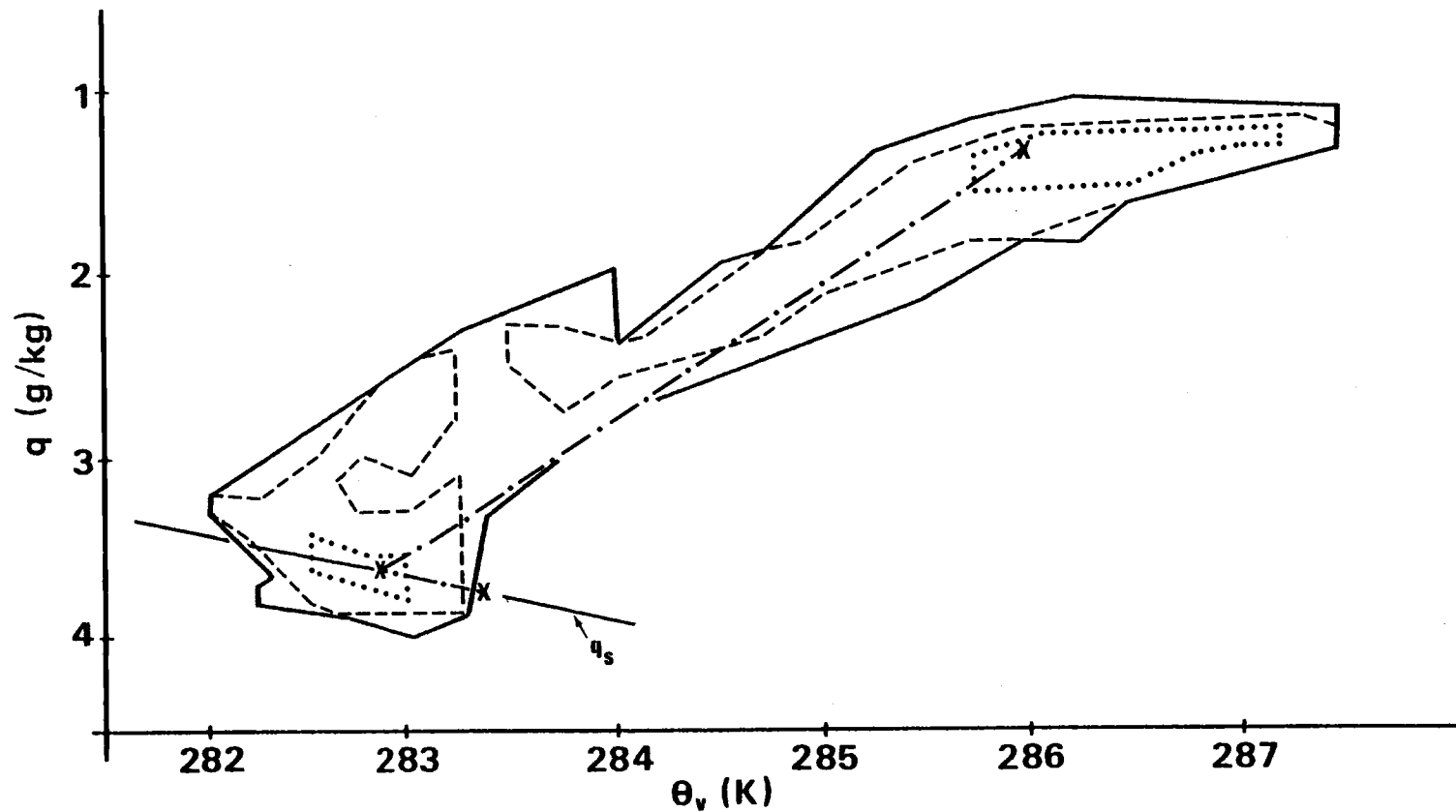


Figure 4a. Joint frequency diagram for the east-west flight. The solid line encloses cells with ten or more observations, the dashed line - 25 or more observations, and the dotted line - 100 or more observations. The total number of observations, N , is 12382. The dot-dash line with the X's is the theoretical entrainment curve; the saturation curve is denoted by q_s .

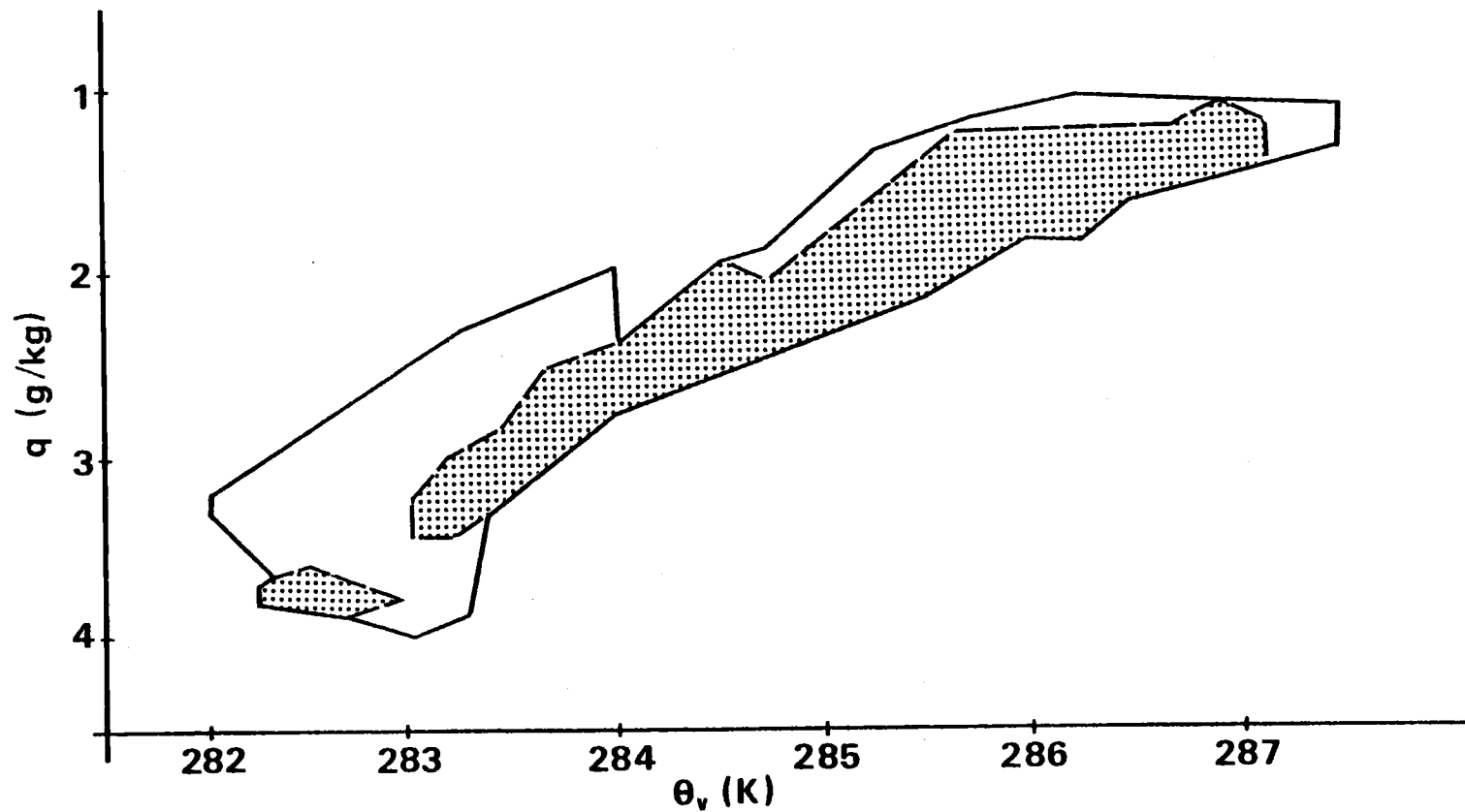


Figure 4b. Joint frequency diagram for segment EW1 where the aircraft flew in and out of the mixed layer. Stippled area represents cells with ten or more observations for the segment. $N = 4100$. Solid outer line is the entire east-west flight.

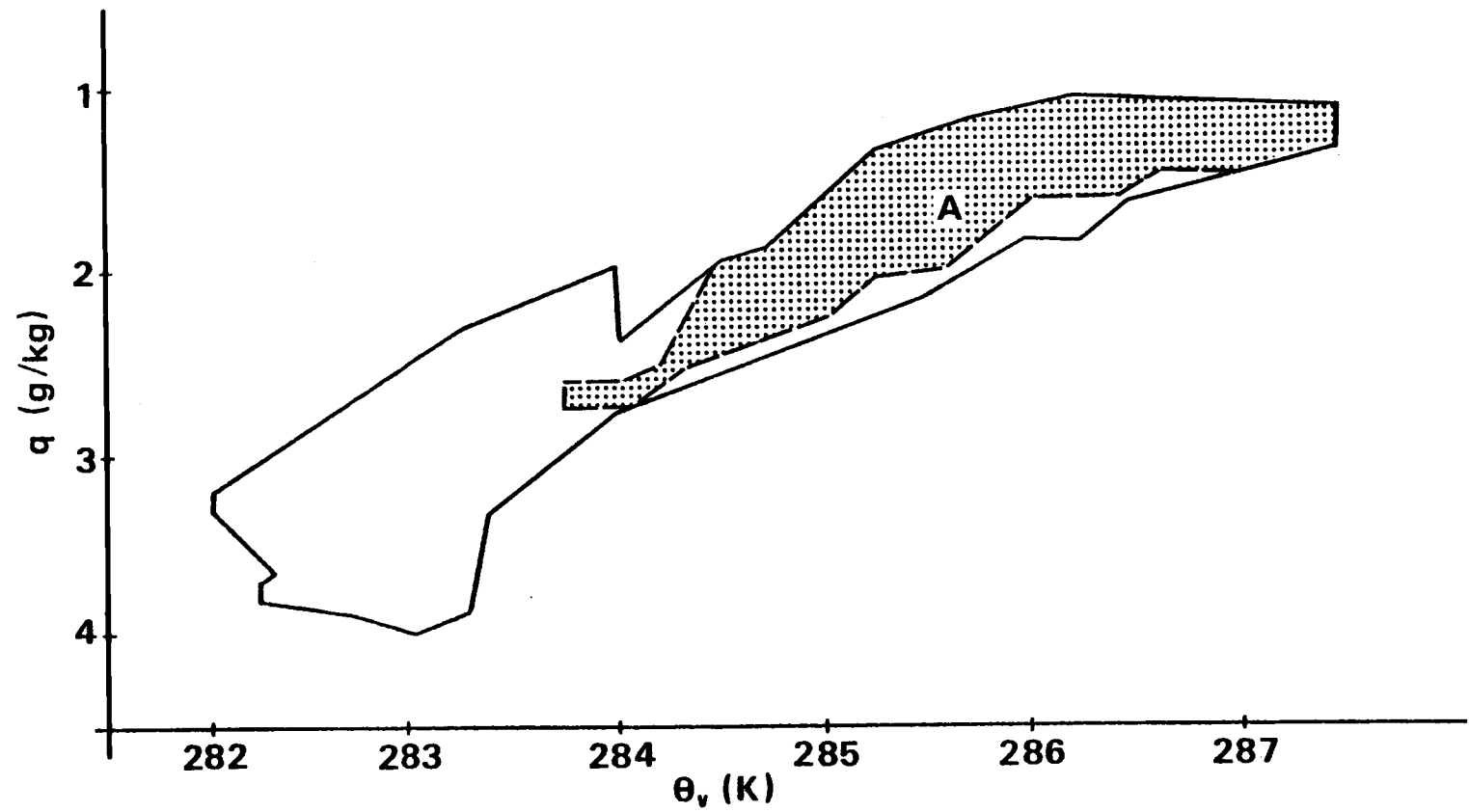


Figure 4c. Same as Figure 4b except for EW2, the free flow segment.

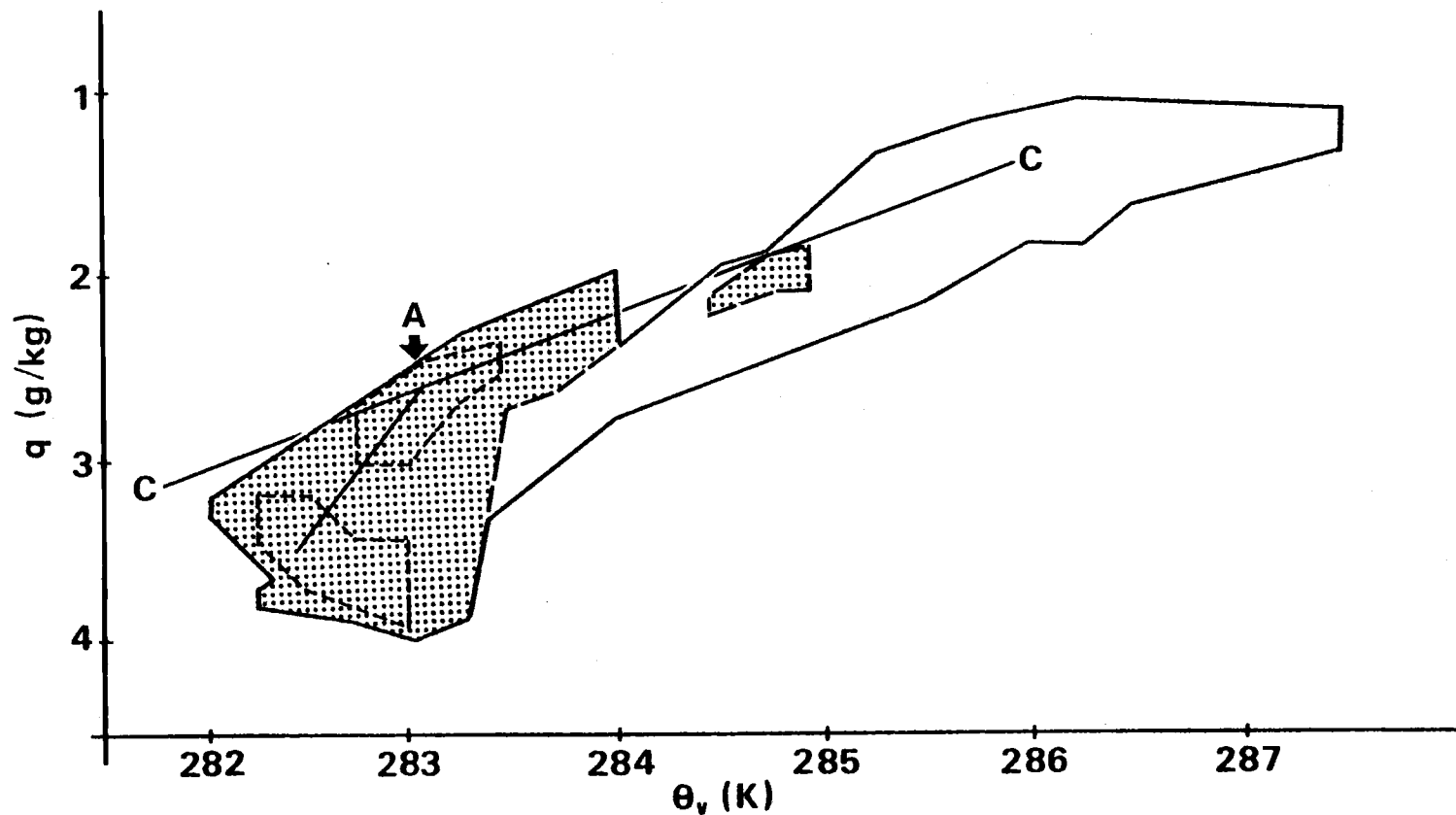
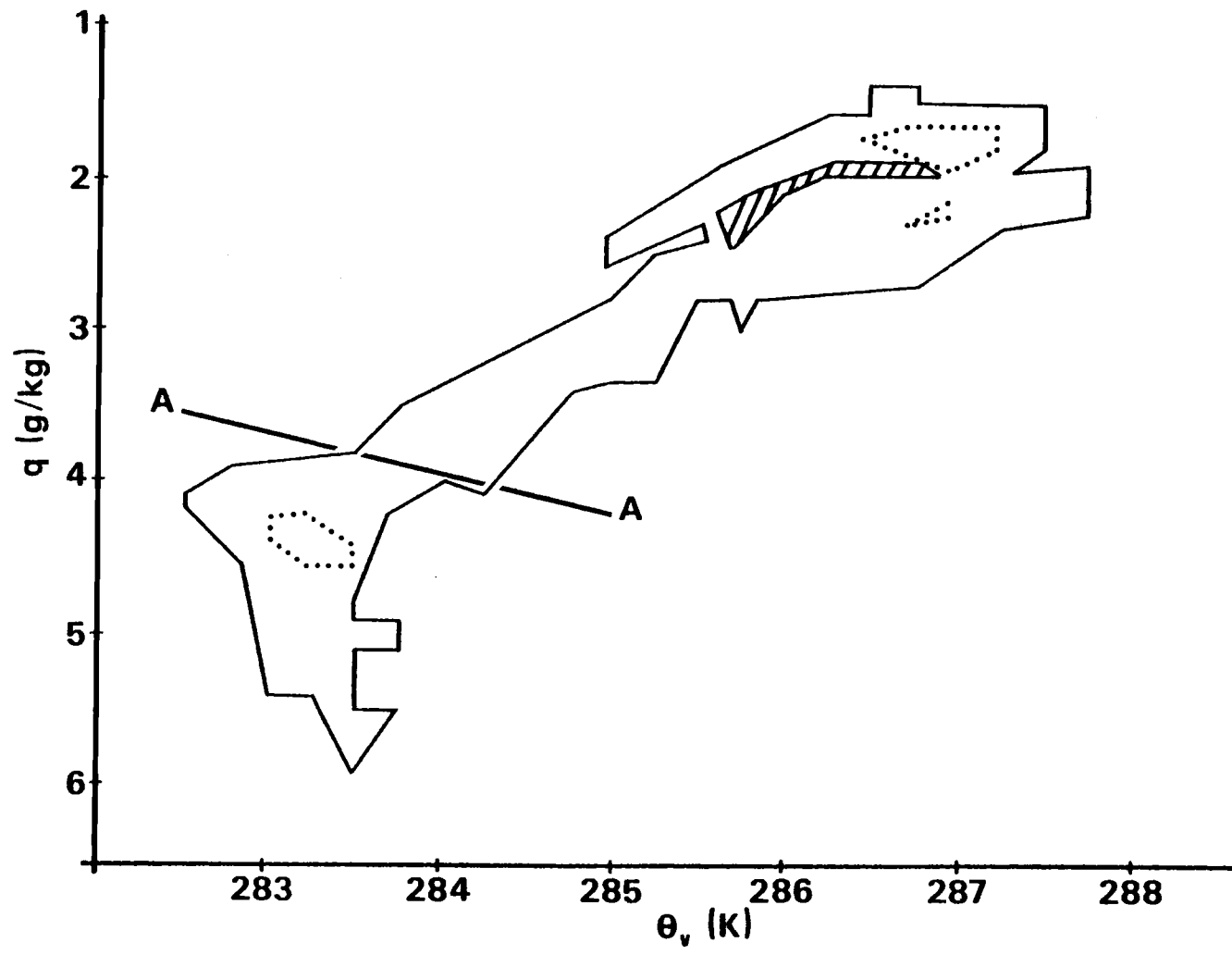


Figure 4d. Same as Figure 4b except for EW3, the mixed layer segment. Dashed line encloses cells with 25 or more observations. Line C-C is the result of a wet-bulb process. Point A is the intersection with a possible entrainment curve.

Figure 5a. Same as Figure 4a except for the entire north-south flight. Line A-A is the saturation curve. Hatched area is a region with less than ten observations.



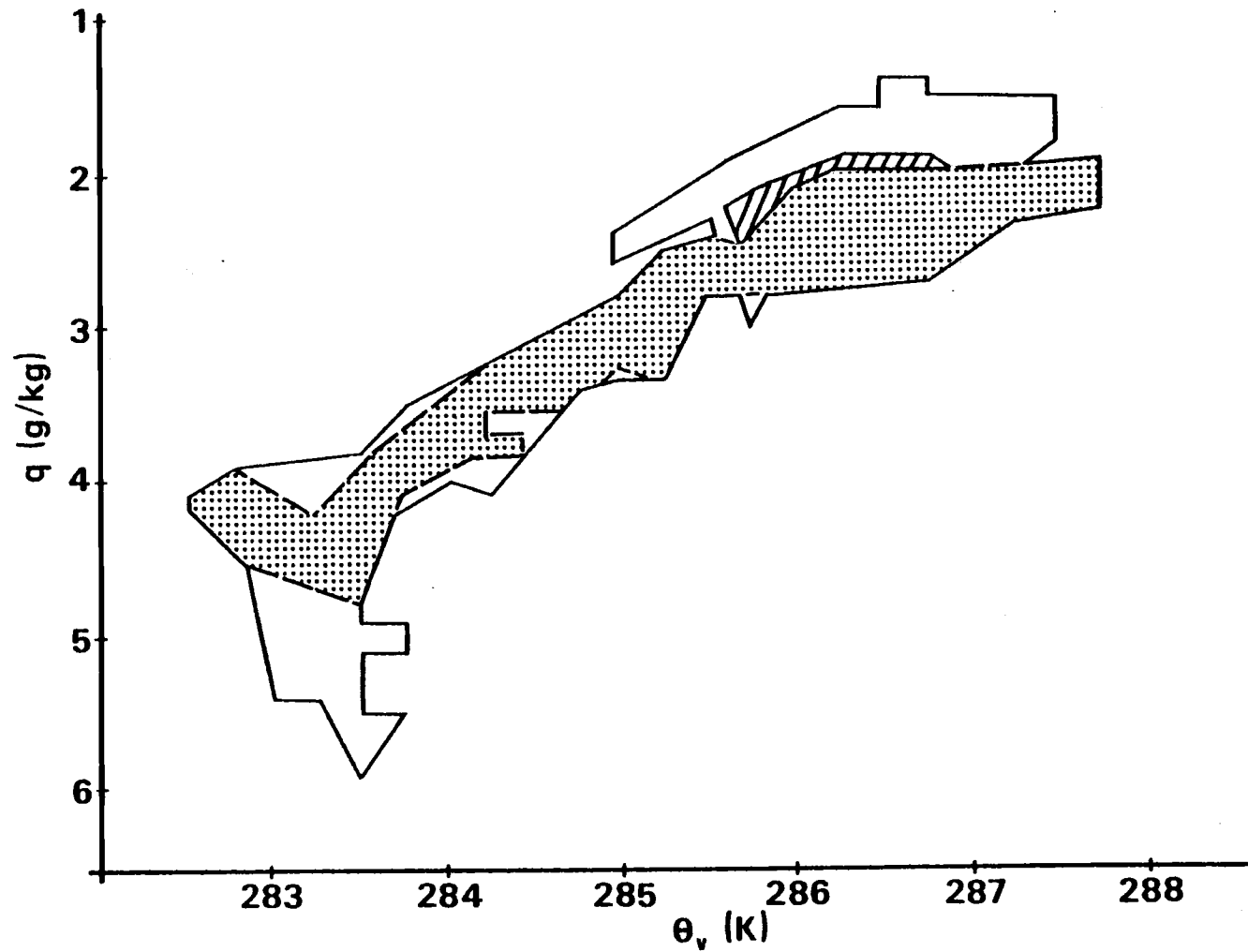


Figure 5b. Joint frequency diagram for segment NS1 where the aircraft flew in and out of the mixed layer. $N = 4200$. Solid outer line is the entire north-south flight.

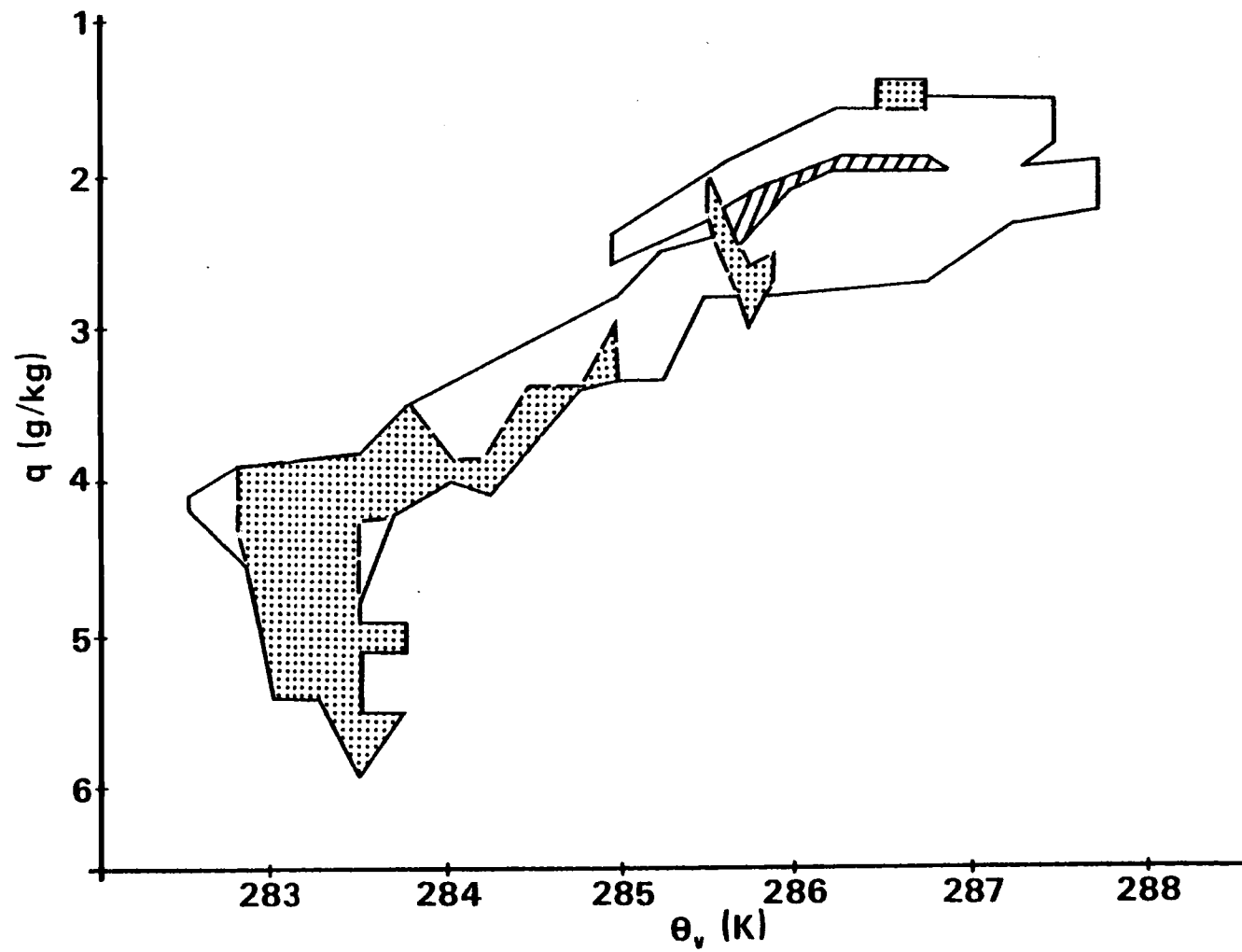


Figure 5c. Same as Figure 5b except for NS2, the mixed layer segment.

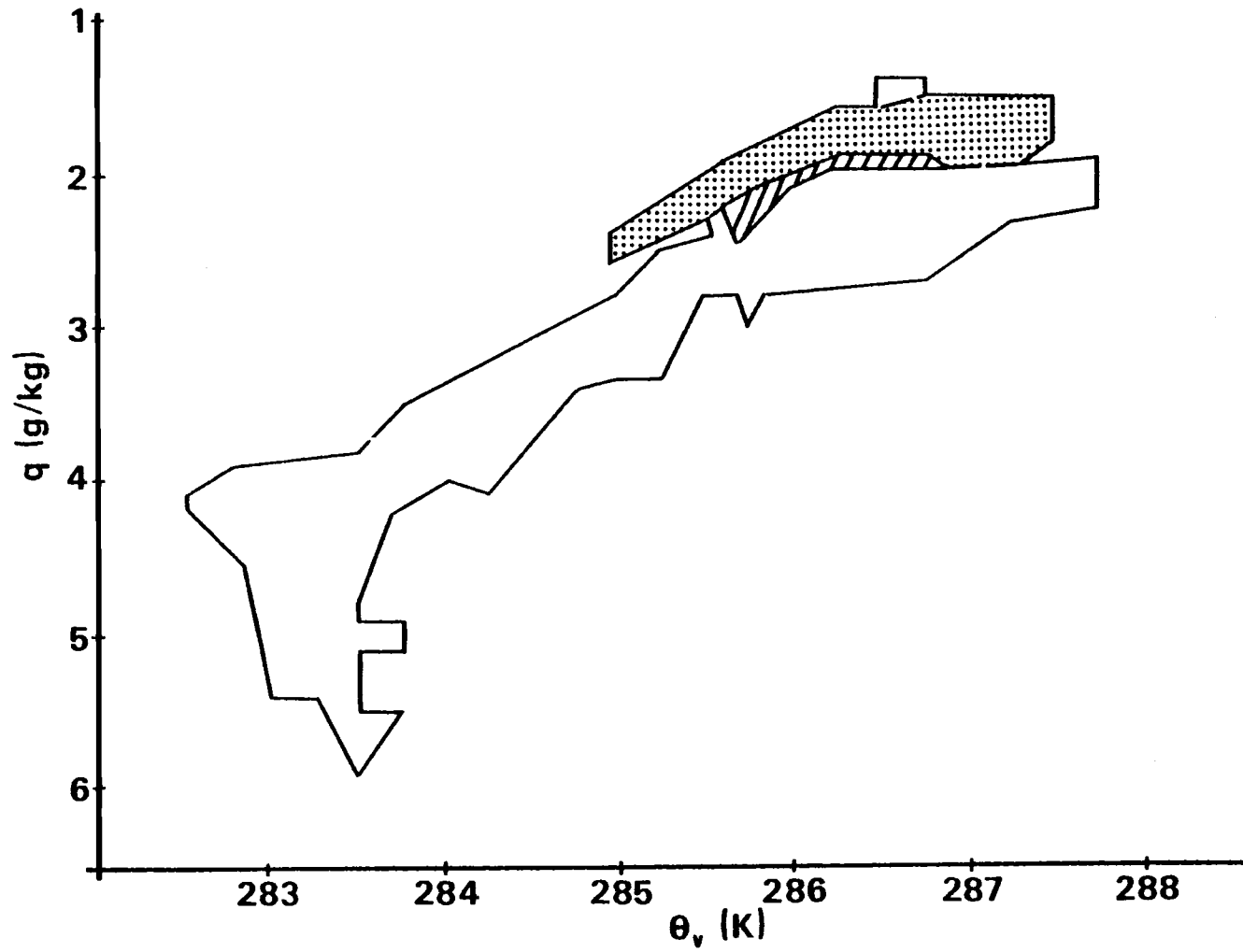


Figure 5d. Same as Figure 5b except for NS3, the free flow segment.

IV. PHENOMENA RELATED TO CEI

We now examine, in a more quantitative manner, some of the atmospheric phenomena that play an important role in the cloud-top entrainment instability. The phenomena of interest are penetrative mixed layer elements (PMLE) and wisps, or dry free flow elements that are engulfed or penetrate into the cloud layer. The term PMLE applies to any mechanism that results in mixed layer air penetrating into the overlying free flow. These elements are not restricted to thermals only and include shear driven eddies and gravity wave updrafts induced by thermals impinging on the inversion. The data used in this study do not allow us to determine which mechanism generate individual PMLE.

Criteria based on one or more of the variables are needed to locate the individual events. Specific humidity, q , is adopted here to select the PMLE and wisps on the EW flight. The criteria used in this study to identify the PMLE are stricter than those used by Mahrt (1981); they are

- 1) $q > 3.0 \text{ gkg}^{-1}$ and increases to at least 3.4 gkg^{-1}
(q increases from unsaturated to saturated air);
- 2) minimum width of 50 m and maximum width of 500 m;
- 3) dry pockets ($q < 3.0 \text{ gkg}^{-1}$) are not wider than 10 m
(to insure that the element is not too dry);
- 4) 60% or more of the environment of the PMLE (1.5 km on each side of the element) is less than 3.0 gkg^{-1} (to isolate the element from air of a similar nature);

- 5) at least a 0.4 gkg^{-1} increase in moisture across the upstream edge.

With these criteria six PMLE are identified.

To locate the wisps, the following requirements are used:

- 1) $q < 3.4 \text{ gkg}^{-1}$ and decreases to at least 3.0 gkg^{-1} ;
- 2) minimum width of 25 m and a maximum width of 500 m;
- 3) moist peaks ($q > 3.4 \text{ gkg}^{-1}$) are not wider than 10 m;
- 4) 60% or more of the element's environment (1.5 km per side) is greater than 3.4 gkg^{-1} .

The rationale for choosing these criteria is similar to that for the PMLE. Twelve wisps are located by these criteria but four are removed from the analysis since they contain other wisps in the near environment (within 1.5 km).

Compositing of the PMLE and wisps was performed, enabling us to study the structure of the "average" wisp or PMLE and its environment, although some of the features may be partially masked by the compositing technique since not all of the elements located are in the same stage of their life cycle and the aircraft does not usually intersect each element at its center. Compositing is done by first dividing each PMLE into 10 equal sections (five for the wisps) and interpolating between points when necessary. Five sections of environmental air are included on each side of the elements. Each section is then averaged over all the PMLE or wisps. The results are shown in Figure 6 for the PMLE. The wisps are divided into five sections since the minimum width is reduced to 25 m to obtain a larger sample and to avoid interpolating twice between two points since the spatial resolution is only 5 m.

A. Composite Penetrative Mixed Layer Elements

Relative rising motion on the upstream side and sinking motion on the downstream side suggest that the mixed layer element rises into the faster moving free flow and is accelerated horizontally by pressure effects associated with the shear (Mahrt, 1981) before sinking back into the mixed layer producing an overturning motion. The shear across the top of the mixed layer has a strong component in the direction of the flight (west to east) and the existence of a turbulent wake at the downstream edge of the PMLE is likely. The wake enhances mixing of PMLE with the drier environmental air, and the occurrence of very cold air at the downstream edge probably results from net cooling (CEI). The cold temperatures in turn lead to strong sinking motion, larger than the sinking produced from an overturning motion.

The strong sinking motion on the downstream side could also be due, in part, to horizontal divergence of the wind (the free flow is moving faster than the cloud air), particularly in the environmental side of the boundary. Divergence, though, cannot explain the colder observed temperatures, thus net cooling and cloud-top entrainment instability seem likely.

The penetrative element with the highest central moisture is plotted in Figure 7. This element probably originated deep within the mixed layer. The high moisture peak suggests that the element was intersected at or very near to its center. The features of this penetrative element are similar to the composite of the six PMLE (which includes this "super-PMLE"), except that the upstream to downstream

differences are accentuated, in part due to the random intersections of the individual PMLE and averaging process. The moisture profile is less symmetric than the profile for the composite PMLE. A large decrease in moisture between upstream and downstream (segments six and 15) indicates that enhanced mixing of mixed layer and environmental air is occurring, probably due to a downstream wake. Strong rising motion of the upstream free flow air is probably in response to encountering the slower moving mixed layer air. Thus the flow is over and around the "super-PMLE", creating an active turbulent wake.

B. Composite Wisp

Figure 8 shows the results of the composite wisp. Evaporative cooling of the temperature probe is a possibility, here, since temperature lags humidity by about one interval (approximately 12 m, here) and the wisps are intersected after extended excursions in cloudy air. If this is the case, the temperature minimum is not as great as shown. The amount of cooling due to the wetting of the sensor probably does not exceed 0.20 K if we consider the temperature observed at interval six of Figure 8 to be anomalously low and assume that the temperature for interval five is the coldest observed. The upstream edge of the wisp (left side of Figure 8) is cooler than the downstream edge by 0.5 K or more. It is likely that this is due to net cooling from the evaporation of cloud droplets.

The cooling on the upstream edge is associated with relative downward motion, perhaps reflecting CEI. Since the upstream edge of the wisp is also the downstream edge of cloud air, this location of

possible CEI is in agreement with previous results. That is, enhanced mixing is expected at the upstream edge of the faster moving wisps. The wisp itself seems to be rebounding, as evidenced by the relative rising motion in the middle sections (seven through nine). This indicates that the wisps may not always be completely entrained.

C. Composite Transitions

The penetrative elements and wisps that have been studied can be considered isolated because of the environmental constraint in the criteria. However, other regions of CEI may occur, and thus moisture jumps in areas where mixed layer and free flow air coexist in more equal proportions were also examined, and jumps from moist-to-dry and dry-to-moist are composited separately. The jumps had to satisfy the following criteria:

- 1) a dry air value of $q < 3.0 \text{ gkg}^{-1}$;
- 2) the moisture jump has to be such that $q > 3.4 \text{ gkg}^{-1}$ within 25 m;
- 3) the dry side of the maximum moisture gradient is defined as the edge;
- 4) no previous PMLE or wisp is included.

Applying these criteria five moist-to-dry and four dry-to-moist moisture jumps were located and composited. The results are shown in Figures 9 and 10. Five points on each side of the maximum moisture gradient are used in the composite (representing 50 m) rather than averages over short segments as in the PMLE and wisp composites.

The moist-to-dry transition represents the downstream edge of

penetrating mixed layer elements and the dry-to-moist transition represents the upstream edge. On the upstream side q and θ_v smoothly increase and decrease, respectively, with no observable minimum in temperature. Relative vertical motions are weak. The cold sinking air at the downstream edge again suggests the existence of cloud-top entrainment instability.

The composites presented in this section suggest the occurrence of net cooling due to evaporation and associated sinking motion and, therefore, cloud-top entrainment instability. To see how the average values compare to all the observations, the composite PMLE and wisp are plotted on the east-west frequency diagram (Figure 11). Each element has a warm edge and a cold edge. The PMLE downstream edge (15) is much colder than the upstream edge (6) and is among the coldest temperatures observed whereas the wisps saturated upstream edge (5) is colder than the downstream edge (11). The cold edge of each is the common edge shared by the PMLE/wisp couplet envisioned in Figure 1.

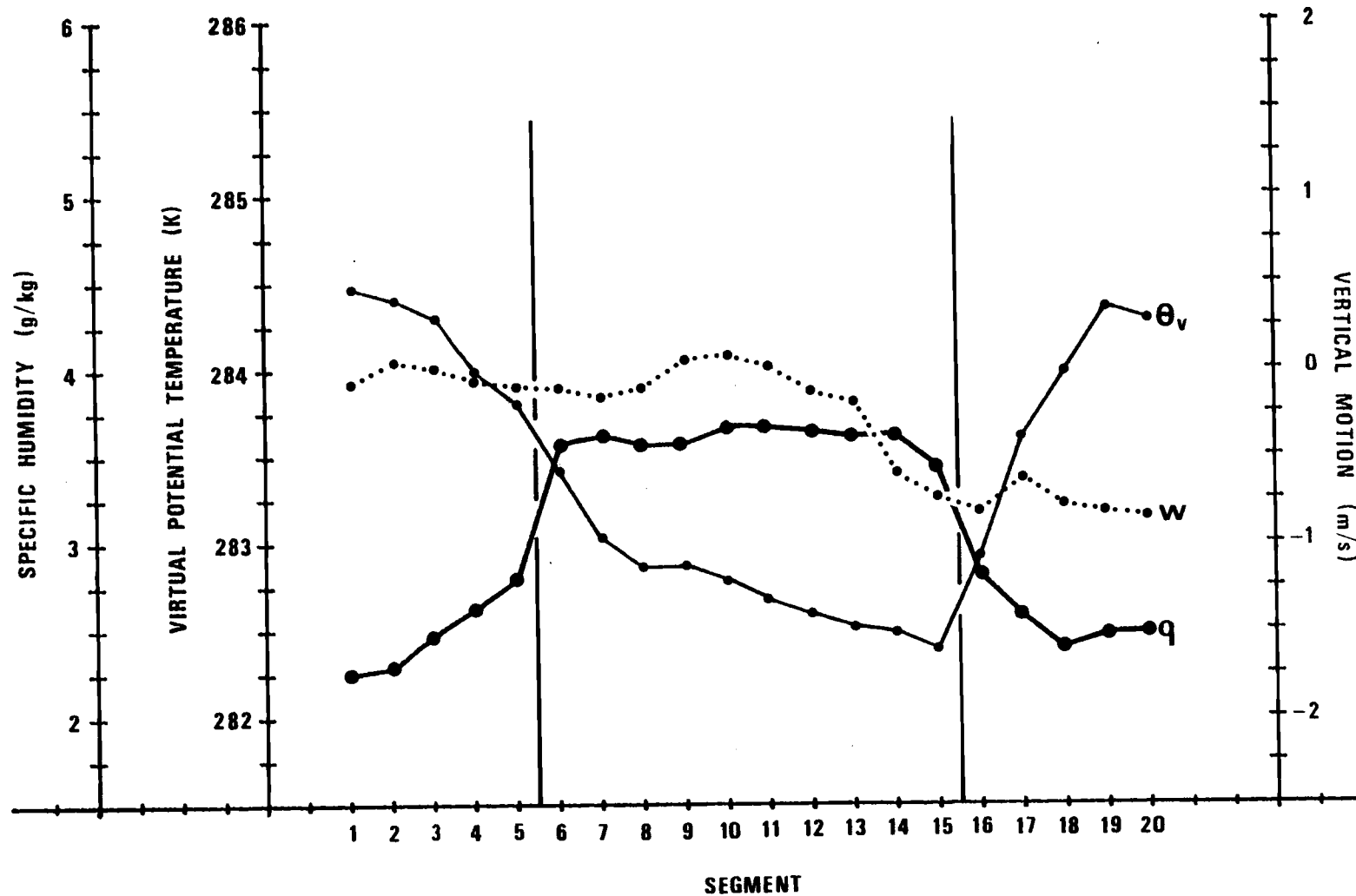


Figure 6. Composite penetrative mixed layer element (six cases). Vertical lines (between 5-6 and 15-16) delineate the boundaries of the element.

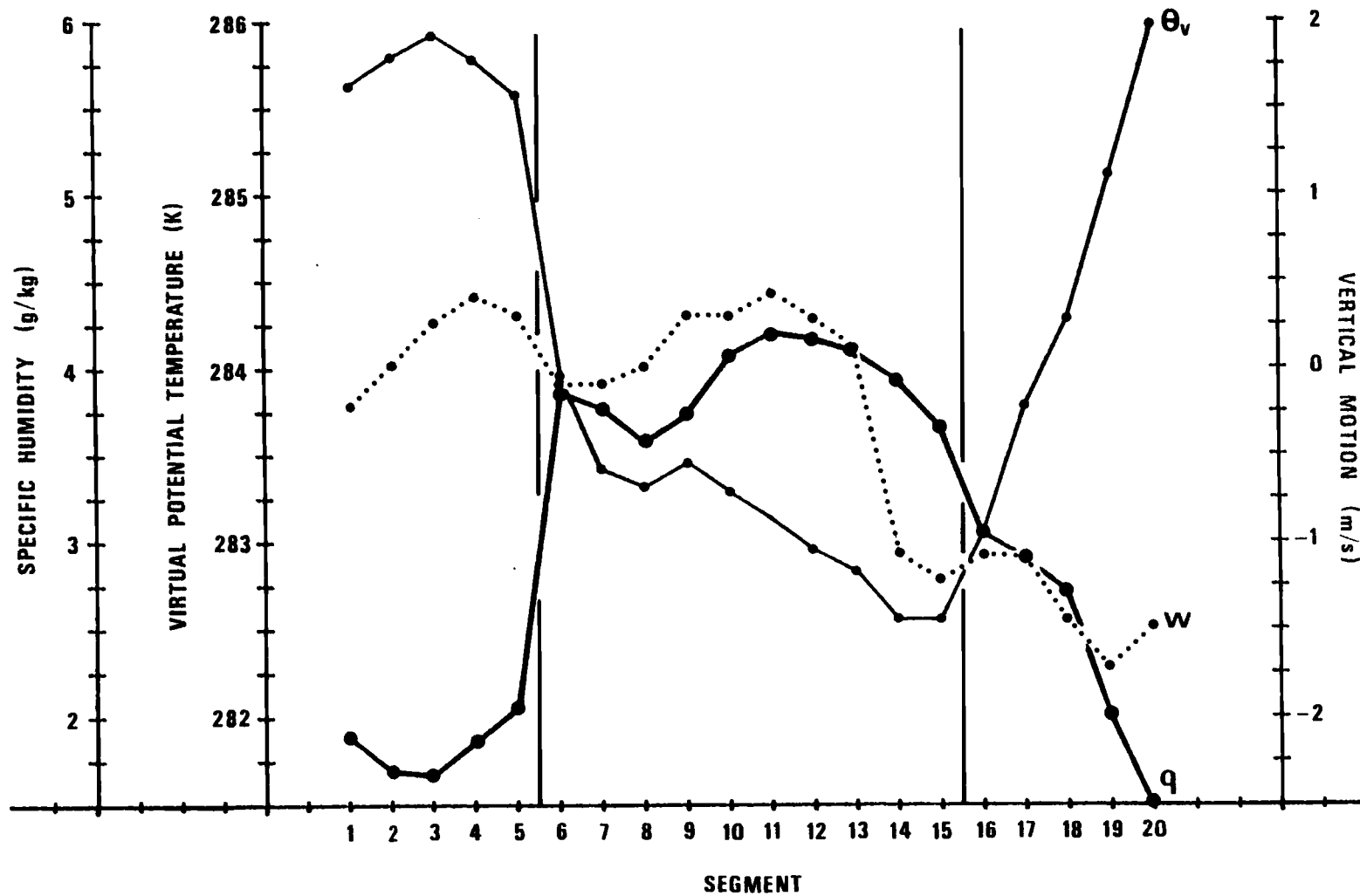


Figure 7. Same as Figure 6 except for penetrative element with the highest moisture value.

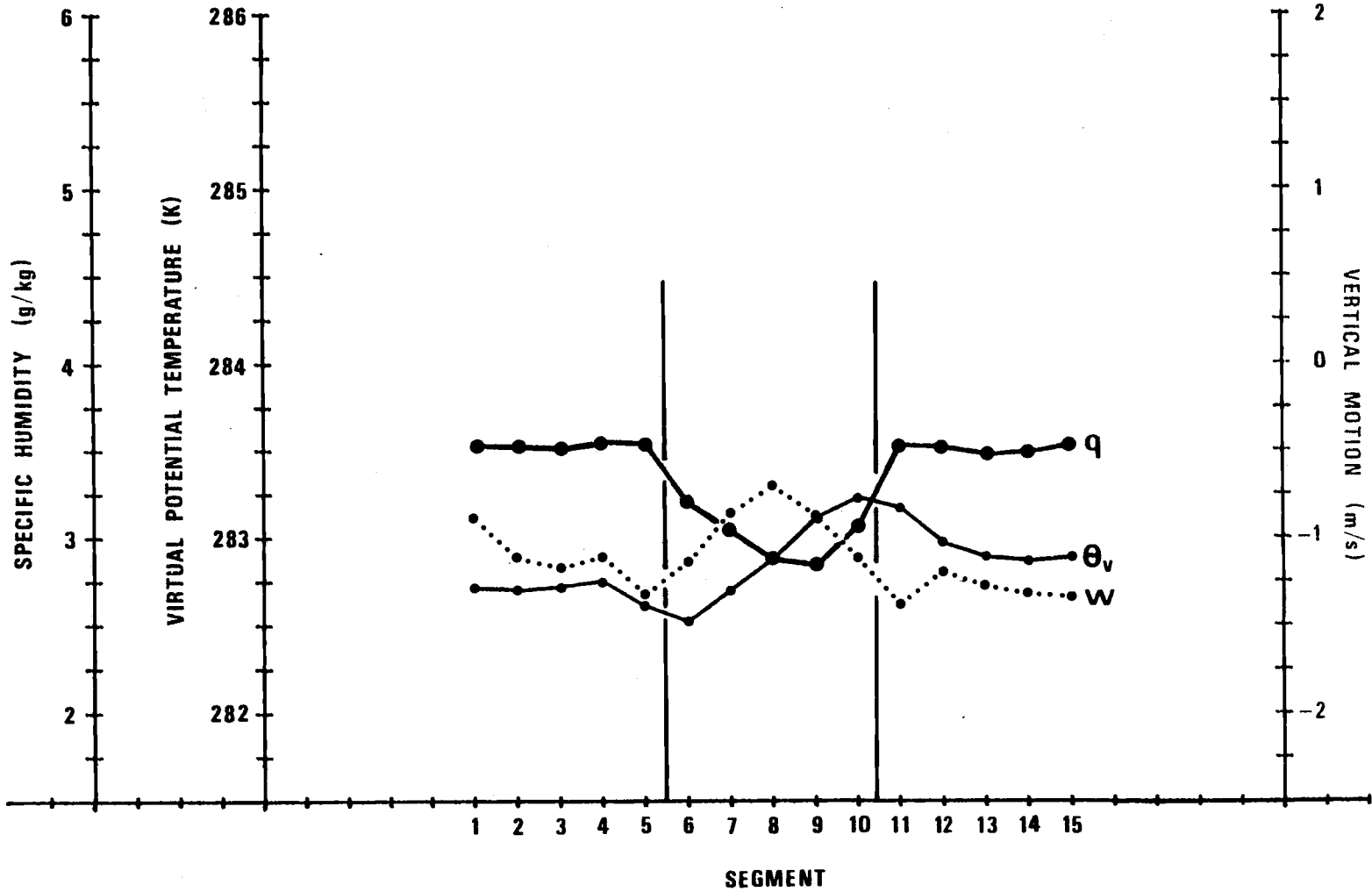


Figure 8. Same as Figure 6 except for wisps (eight cases).

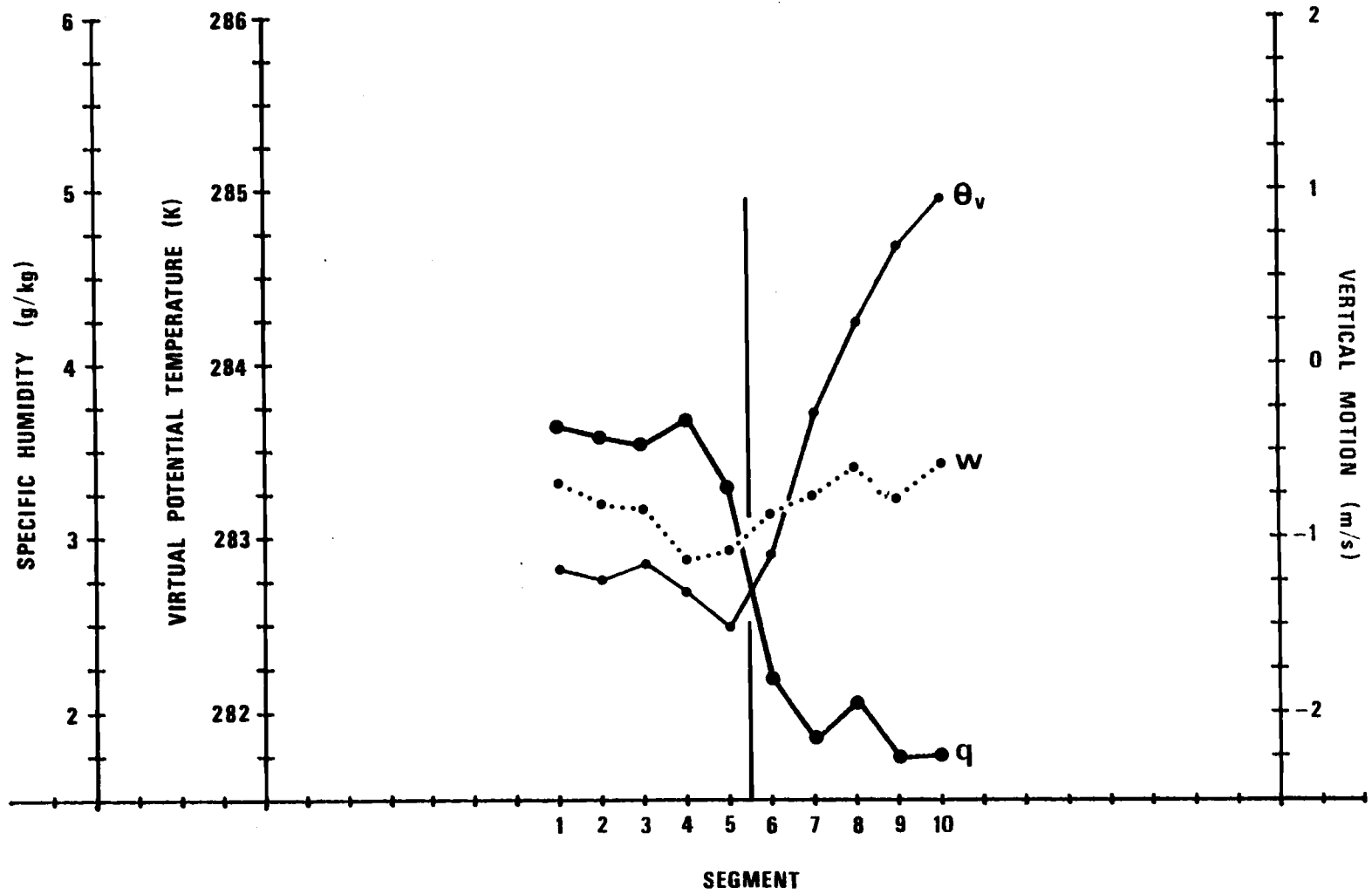


Figure 9. Composite of downstream moist-to-dry transitions (five cases).

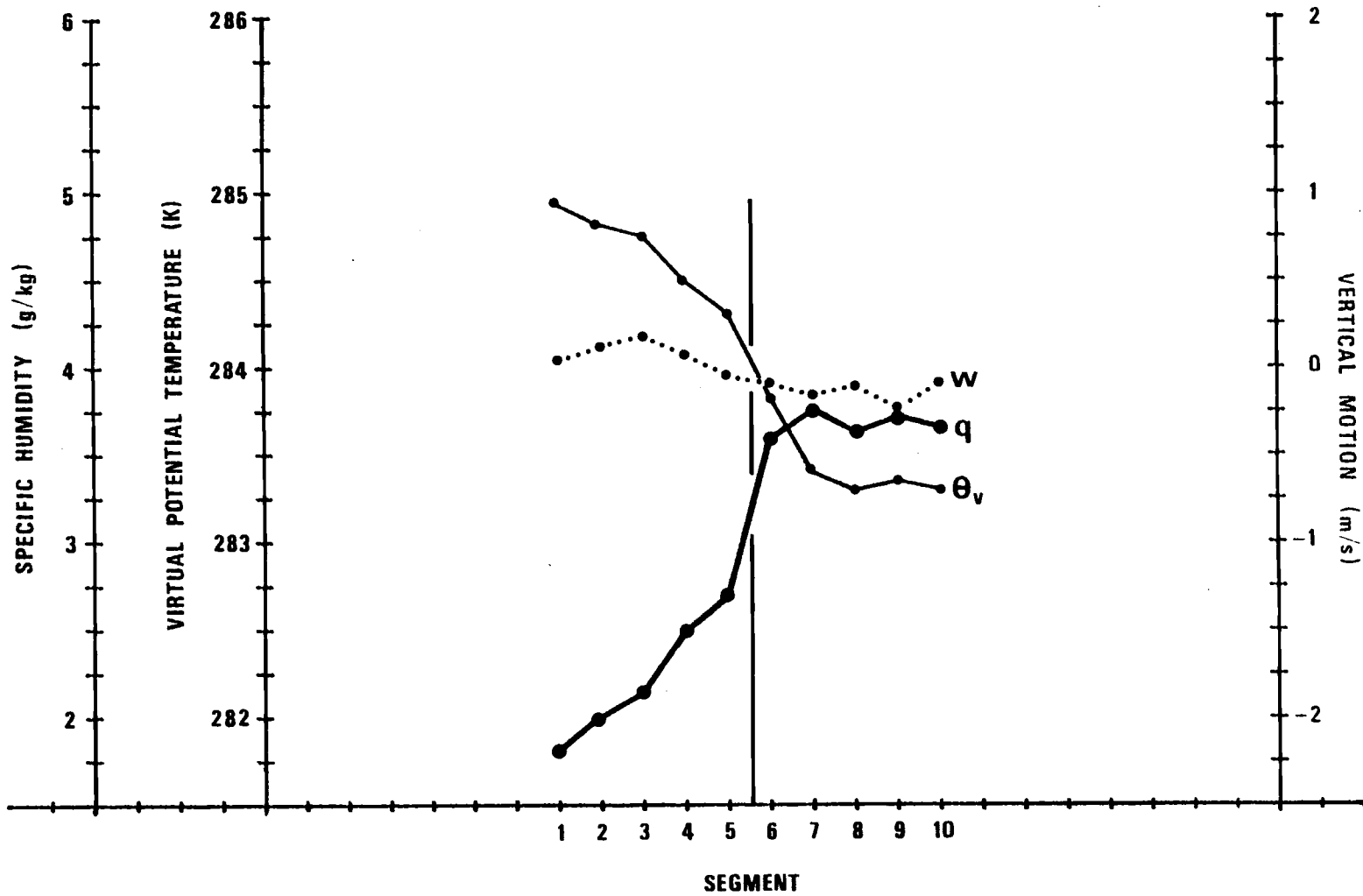


Figure 10. Composite of upstream dry-to-moist transitions (four cases).

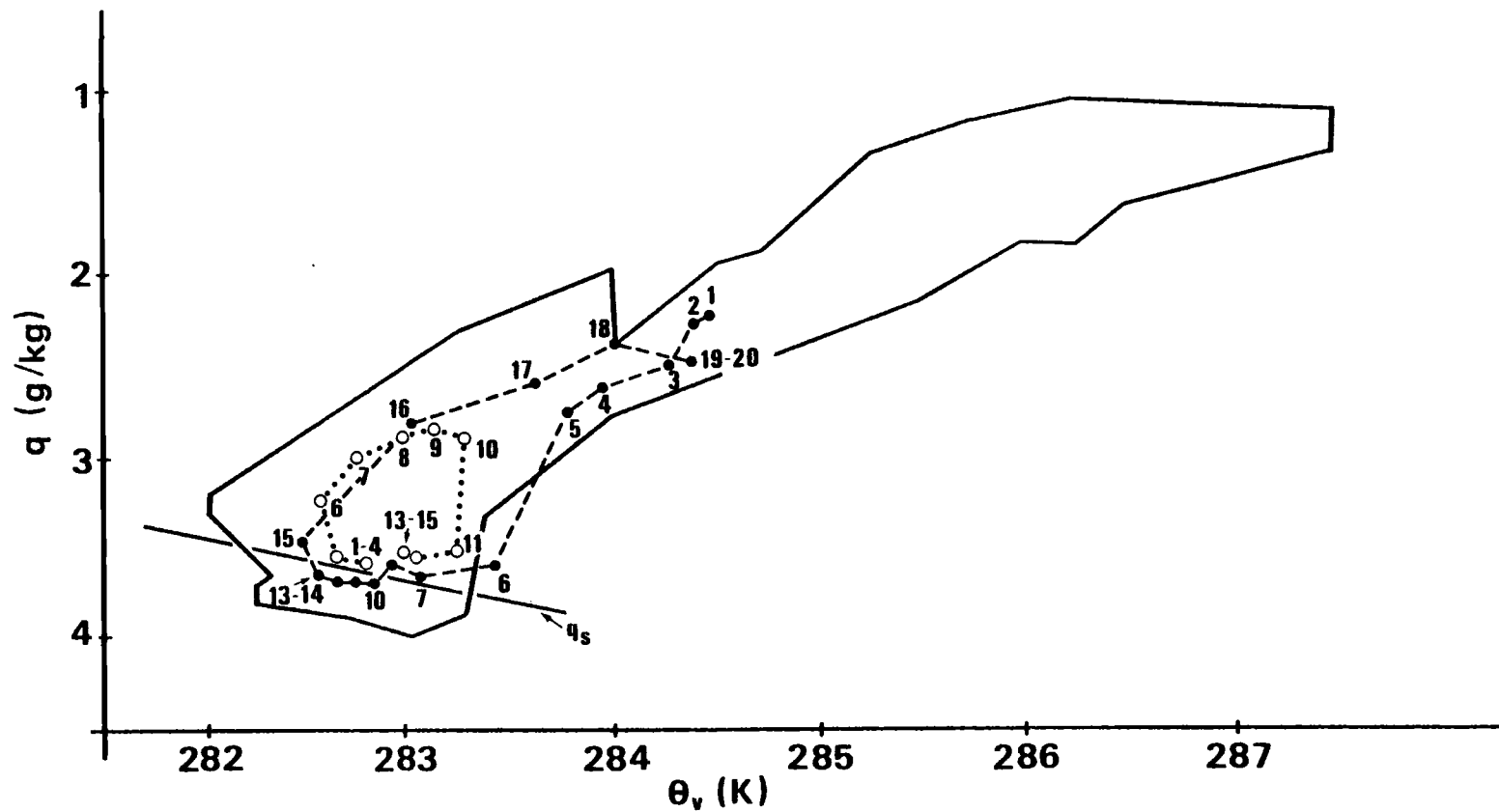


Figure 11. The east-west frequency diagram with the composite PMLE (●) and wisp (○) plotted. The numbers refer to the segment in Figures 6 and 8. The saturation curve is indicated by q_s .

V. SUMMARY

From observations at the top of the cloud-topped mixed layer, evidence for cloud-top entrainment instability is presented. Joint frequency diagrams of humidity and temperature indicate that this mechanism exists and occurs on a scale of about 50 km. The configuration of observations in these diagrams is characteristic of the mixing of a free flow parcel in a cloud. This results in a drying of the mixture and a net cooling due to evaporation exceeding the entrainment of sensible heat. Once all the liquid water is evaporated, the mixture warms and continues to dry with additional mixing with free flow air.

Anomalously cold temperatures observed in a flight subsegment may be due to water droplets diffusing into the free flow near the cloud. The parcel then undergoes a wet-bulb process that reduces the temperature of the parcel. Before completing the wet-bulb process, i.e., before the parcel reaches saturation, the parcel is entrained into the cloud where cloud-top entrainment instability may occur.

The record for the east-west flight is systematically searched for penetrative mixed layer elements (PMLE) and wisps (free flow air penetrating into the cloud). The PMLE and wisps are composited, producing an "average" PMLE and wisp. The composites show a net cooling and associated sinking motion due to evaporation on the downstream side of PMLE and on the upstream side of wisps. These results suggest the interaction among shear, PMLE and wisps and the existence of cloud-top entrainment instability.

Future observational studies of cloud-top entrainment instability should include the effect of liquid water content. The diagrams presented here, for example, can then be adjusted to account for the liquid water, enabling a more accurate determination of entrainment curves and assessment of the occurrence of CEI. In addition the inclusion of longwave and shortwave radiation measurements at two levels at cloud top would allow the importance of radiative cooling relative to evaporative cooling to be determined.

VI. BIBLIOGRAPHY

- Ball, F. K., 1960: Control of inversion height by surface heating. Quart. J. Roy. Meteor. Soc., 86, 483-494.
- Browning, K. A., J. R. Starr and A. J. Whyman, 1973: The structure of an inversion above a convective boundary layer as observed using high-power pulsed doppler radar. Bound.-Layer Meteor., 4, 91-111.
- Carson, D. J., and F. B. Smith, 1974: Thermodynamic model for the development of a convectively unstable boundary layer. Adv. Geophysics, 18A, Academic Press, 462 pp.
- Deardorff, J. W., 1974: Three-dimensional numerical study of the height and mean structure of a heated planetary boundary layer. Bound.-Layer Meteor., 7, 81-106.
- _____, 1976: Usefulness of liquid-water potential temperature in a shallow cloud model. J. Appl. Meteor., 15, 98-102.
- _____, 1980: Cloud top entrainment instability. J. Atmos. Sci., 37, 131-147.
- Goisa, N. I., and V. M. Shoshin, 1969: Eksperimental'naia model' radiatsionnogo rezhima "srednego" sloistoobraznogo oblaka. [Experimental model of the radiation regime of an average stratiform cloud]. Kiev, Ukraine. Nauchno-Issledovatel'skii Gidrometeorologicheskii Institut, Trudy, No. 82, 28-41.
- Grant, D. R., 1965: Some aspects of convection as measured from aircraft. Quart. J. Roy. Meteor. Soc., 91, 268-281.
- Heymsfield, A. J., J. E. Dye and C. J. Biter, 1979: Overestimates of entrainment from wetting of aircraft temperature sensors in cloud. J. Appl. Meteor., 18, 92-95.
- Jensen, N. O., and D. H. Lenschow, 1978: An observational investigation of penetrative convection. J. Atmos. Sci., 35, 1924-1933.
- Lenschow, D. H., 1972: The Air Mass Transformation Experiment (AMTEX): A report of the AMTEX study conference, November 10-13, 1971, Tokyo, Japan. Bull. Amer. Meteor. Soc., 53, 353-357.
- _____ and E. M. Agee, 1976: Preliminary results from the Air Mass Transformation Experiment (AMTEX). Bull. Amer. Meteor. Soc., 57, 1346-1355.
- _____ and P. L. Stephens, 1980: The role of thermals in the convective boundary layer. Bound.-Layer Meteor., 19, 509-532.

- Lilly, D. K., 1968: Models of cloud-topped mixed layers under a strong inversion. Quart. J. Roy. Meteor. Soc., 94, 292-309.
- Mahrt, L.J., 1981: Circulations in a sheared inversion layer at the mixed layer top. To appear in J. Meteor. Soc. Japan.
- Murray, F. W., and L. R. Koenig, 1972: Numerical experiments on the relation between microphysics and dynamics in cumulus convection. Mon. Wea. Rev., 100, 717-732.
- Ninomiya, K., 1976: Note on the synoptic situation of AMTEX '75. J. Meteor. Soc. Japan, 54, 334-337.
- Palmer, S. G., S. J. Caughey and K. W. Whyte, 1979: An observational study of entraining convection using balloon-borne turbulence probes and high power doppler radar. Bound.-Layer Meteor., 16, 261-278.
- Paltridge, G. W., 1974: Atmospheric radiation and the gross character of stratiform cloud. J. Atmos. Sci., 31, 244-250.
- Randall, D. A., 1980: Conditional instability of the first kind upside-down. J. Atmos. Sci., 37, 125-130.
- Reed, R. J., 1960: Principal frontal zones of the northern hemisphere in winter and summer. Bull. Amer. Meteor. Soc., 41, 591-598.
- Roach, W.T., and A. Slingo, 1979: A high resolution infrared radiative transfer scheme to study the interaction of radiation with cloud. Quart. J. Roy. Meteor. Soc., 105, 603-614.
- Stephens, G. L., G. W. Paltridge and C. M. R. Platt, 1978: Radiation profiles in extended water clouds. III: Observations. J. Atmos. Sci., 35, 2133-2141.
- Stull, R. B., 1976: Mixed-layer depth model based on turbulent energetics. J. Amer. Sci., 33, 1268-1278.
- Tetens, O., 1930: Uber einige meteorologische Begriffe. Zeitschrift fur Geophysik, 6, 297-309.
- Wyngaard, J. C., W. T. Pennell, D. H. Lenschow and M. A. LeMone, 1978: The temperature-humidity covariance budget in the convective boundary layer. J. Atmos. Sci., 35, 47-58.
- Zdunkowski, G. W., G. C. Korb and C. T. Davis, 1974: Radiative transfer in model clouds of variable and height constant liquid water content as computed by approximate and exact methods. Contr. Atmos. Phys., 47, 157-186.